ISSN 0915-633X

NATIONAL INSTITUTE FOR FUSION SCIENCE

Theoretical and Experimental Studies on Electric Field and Confinement in Helical Systems

H. Sanuki, K. Itoh, J. Todoroki, K. Ida, H. Idei,
H. Iguchi and H. Yamada

(Received - June 7, 1994)

NIFS-286 June 1994

RESEARCH REPORT
NIFS Series

NAGOYA, JAPAN

Theoretical and Experimental Studies on Electric Field and Confinement in Helical Systems

H. Sanuki, K. Itoh, J. Todoroki
K. Ida, H. Idei, H. Iguchi and H. Yamada

National Institute for Fusion Science
Nagoya, 464-01, Japan

This article is prepared for the presentation
at
the Workshop on Transport in Fusion Plasmas
Aspënas, Göteborg, Sweden, June13-16, 1994

Abstract

The present study consists of two parts. The first part is oriented to a theoretical model of selfconsistent analysis to determine simultaneously the electric field and loss cone boundary in heliotron/torsatron configurations under the influence of nonclassical particle losses. The second part is refered to the analysis on NBI heated and ECH plasmas in Compact Helical System (CHS) device. A comparison is made between theoretical results and experimental observations.

Keywords: radial electric field, theoretical model, experimental observations, NBI and ECH plasmas, neoclassical and nonclassical losses

1 Introduction

An important role of the electric field and/or plasma rotation on the suppression of microinstabilities and the improved plasma confinement has been widely recognized in various devices with different configurations, sizes and plasma parameters. The experimental observations in tokamaks[1)~4)] as well as stellarators[5),6)] have provided the database for an increased understanding of the physics associated with radial electric field, showing that the radial profiles of plasma rotation (electric field) are different for L−mode and H−mode operations, respectively. Various theoretical models[7)~10)] have been proposed and predicted the structural change of radial electric field in connection with L/H transition. Although many works have been done up to now, the complete comparison of results between theories and experiments is far from sufficient, because of the diagnostic and theoretical difficulties. High spatial- and time- resolved measurements of plasma parameters are required for investigations of improved plasma confinement such as the H−mode. Recent considerable progress on both the theoretical modelling and the measurement techniques such as the charge exchange recombination spectroscopy (CXRS), heavy ion beam probing (HIBP) and laser bow-off Lithium beam probing, may realize the detailed analysis of electric field profile in the whole plasma region and its influence on improved plasma confinement. There are several fundamental questions whether the electric field always be a useful tool from the confinement improvement, and the spontaneous electric field in plasma is sufficient or any specific idea to control the electric filed is needed. To reply these questions, an understanding of physical process on cooperative phenomena associated with electric field in plasma should be deepened.

In heliotron/torsatron and stellarators, the relationship among the electric filed, fluctuations and plasma confinement actively have been studied in the past[11)~13)] and existing [14)~17)] devices. Particularly, the Compact Helical System (CHS) experiment, in which the electric field profile in the whlole plasma region can be evaluated from both toroidal and poloidal rotation velocities and pressure gradient by using the CXRS measurement data, really encourages the study on the electric field generation mechanism and its fine structure[18),19)] These are the data-base to investigate the influence of electric field on the confinement improvement.

The purpose of the present study is to discuss a theoretical model to determine the electric field in heliotron/torsatron and an understanding of the cooperative mechanism among the electric field, loss of energetic particles and confinement characteristics. A flow chart of mutual relations of typical cooperative phenomena involved in the present analysis is sketched in Fig. 1. In general, the electric field in plasmas is determined by balancing the driving forces with the drag forces. There are essentially two type of forces to drive plasma rotations : one is the force associated with momentum transport due to, for example neutral beam injection (NBI) and the other is the bipolar fluxes caused by electron and ion diffusions. Also, several approaches for the active control of a radial electric field have been discussed, which are by driving plasma rotation with neutral beam injection into the plasma, by controlling ion and elctron losses with NBI or electron cyclotron heating (ECH), due to biasing (electrode, limiter, divertor, etc.), and so on. Typical processes involved in the recent CHS experiments are also shown in Fig. 2.

We have discuss the physical mechanism of the generation and structure of E_r in NBI and ECH plasmas in CHS. Comparison between theoretical prediction and experimental observation has also been made.

2 Theoretical Model to determine E_r

The radial electric field in the steady state is evaluated by the ambipolarity equation

$$\Gamma_i = \Gamma_e \tag{1}$$

where Γ is the radial particle flux and suffix e and i denote electrons and ions, respectively. Taking into account nonclassical terms, we write Γ_i and Γ_e as

$$\Gamma_i = \Gamma_i^{NC} + \Gamma_i^{orbit} + \Gamma_{fcx} + \Gamma_{icx} + \Gamma_{i,a} \ , \tag{2}$$

$$\Gamma_e = \Gamma_e^{NC} + \Gamma_{e,a} + \Gamma_{RF} \ . \tag{3}$$

These equations consist of the neoclassical fluxes (denoted by the subscript NC), the direct ion orbit loss flux (Γ_i^{orbit}), the charge exchange contributions of fact ions (Γ_{fcx}) and bulk ions (Γ_{icx}), and that driven by anomalous transport (Γ_a). The explicit forms of these fluxes are discussed in literatures[20),21)] which are summarized as

$$\Gamma_i^{orbit}(r) = [P(r) - P(r_*)]/4\pi^2 r R W_b \ , \tag{4}$$

$$\Gamma_{fcx} = (M_f n_f n_o / eB_p) < \sigma_{cx} v > v_f \ , \tag{5}$$

$$\Gamma_{i,cx} = (M n_i n_o T_i / e^2 B^2) < \sigma_{cx} > \times [Ze\frac{E_r}{T_i} - \{1 + \eta_i(\mu_{i1}/\mu_{i2}\} n_i'/n_i] \ . \tag{6}$$

In Eqs. (4)~(6), $P(r)$ is the input power crossing the minor radias r, W_b denotes the beam energy, r_* the radius representing the loss boundary, $M_f(M)$ the fast (bulk) ion mass, $n_f(r)$ the fast ion density, $< \sigma_{cx} >$ the charge-exchange cross section, and μ_{i1} and μ_{i2} are neoclassical viscosity coefficients. As for the anomalous flux (Γ_a) is concerned, we here assume the functional form of the bipolar part of anomalous flux, $\Delta\Gamma_a \equiv \Gamma_{i,a} - \Gamma_{e,a}$ in the form

$$\Delta\Gamma_a = -\alpha_A(\partial n/\partial r)/n \ , \ \alpha_A = const \ . \tag{7}$$

Here, the coefficient α_A is the parameter, which is evaluated roughly by using experimental data of particle transport based on steady state density profile and neutral particle behavior[22)] Γ_{RF} denotes the RF-induced flux, which will be discussed later.

The radial electric field in the steady state is evaluated by the ambipolarity equation (1). But we must solve not only E_r but also loss cone boundary simultaneously because of the dependence of the radius r_* in Eq. (4) on the radial electric field, $r_*[E_r]$. Once E_r and r_* are determined, we can evaluate the power partition among the shine-through, direct orbit loss, charge exchange loss and bulk heating. The explicit formula is discussed in Ref. [21]. These evaluations may be important to conclude the overall trade-off on the energy balance.

3 Machine and Plasma Parameters in CHS

The Compact Helical System (CHS) is a heliotron/torsatron device with a pole number of $l = 2$, a toroidal period number $m = 8$ and an aspect ratio of 5. The magnetic field configuration of this type of device has flexibility because it is controllable by adjusting the poloidal field coil currents. The major machine parameters and typical plasma parameters for the NBI and NBI + ECH experiments in CHS are summarized in Table 1.

The electron temperature and density profiles are measured with Thomson seattering. The ion temperature and poloidal as well as toroidal rotation velocity profiles, are measured by the CXRS. The neutral density profile is also evaluated by a laser-induced fluorescence technique[23] For the distributions for fast particles and neutral particles, we choose a model distribution as

$$n_0(\rho) = n_{0s} exp[-\alpha_0(1-\rho)^2] , \tag{8}$$

$$n_f(\rho) = n_{0f} exp[-\alpha_f \rho^2] . \tag{9}$$

where $\rho = r/a$ and the suffix 0 and f denote the neutral and fast particles, respectively, and coefficients α_0 and α_f are assumed to be constant. We here take $\alpha_0 \simeq 10$ and $\alpha_f \simeq 2$, modelling the broad fast ion profile and reproducing the profile of neutral density as shown in Ref. [23].

4 Radial Electric Field in NBI Heated Plasmas

The radial electric field has been measured in the NBI heated plasma in the CHS device[18] To study the dependence of collisionality on E_r, two typical discharges, namely, the low and high density NBI experiments were carried out by adjusting gas-puffing with NBI power fixed to be 1MW. The neutral beam injection angle is almost tangential for both cases. The NBI heating experiment with variable injection angle has also been done to study the effect of fast ion orbit loss on the radial electric field E_r.

Radial electric field profile is evaluated from the experimental data such as $n_e(r), T_e(r)$, $T_i(r), U_\vartheta$ and U_ϕ with use of momentum balance equation

$$E_r = (\partial P_I/\partial r)/eZ_I n_I - (B_\vartheta U_\phi - B_\phi U_\vartheta) . \tag{10}$$

In order to explain the generation mechanism of the radial electric field, we determine E_r from the ambipolarity equation (1) with Eqs. (2) $\sim$ (6). As was studied in the previous paper[18] the quantitative comparison between the neoclassical results and experimental observations on E_r profile was far from satisfactory for both typical low (A) and high (B) density NBI discharges. Sample distributions of density, temperature and observed E_r profile are shown in Fig. 3, together with the neoclassical results. It was found from the comparison that the experimentally observed E_r deviates from the neoclassical predictions. Therefore, some other large ion loss process is required to explain this discrepancy.

We here discuss the effects on E_r, which come from the loss cone loss of fast ions, the loss of fast ions through charge exchange with neutrals, and an anomalous loss[21]

4.1 Effect of fast ion orbit loss

We first study the effect of fast ion orbit loss on E_r, for given parameters of density and temperatures shown in Fig. 3. In these studies, we use analytic formulas[24] which describe the relation between E_r and the minimum energies of particles entering the loss cone, together with the ambipolarity relation (1). For simplicity, we also assume that the particles are lost if they reach the outermost magnetic surface. By determining the loss boundary r_* selfconsistently, we obtain the radial profiles of E_r, which are shown in Fig. 4 (A) for low density and in Fig. 4 (B) for high density, respectively. These results show that the fast ion loss flux caused by the loss cone makes E_r more negative but the influence of the orbit loss appears only in the plasma edge. These theoretical predictions have been confirmed in the NBI heating experiment with variable injection angle[25] Some other ion loss process in addition to orbit loss, which is several times as large as the neoclassical loss, is necessary in the region of $0.5a < r < 0.8a$ to explain the discrepancy between theoretical results and experimental observations.

4.2 Effect of neutral particles

The neutral hydrogen profile in the core plasma region and the toroidal/poloidal distributions in the recycling area near the inner wall are measured by using a calibrated TV camera and a laser-induced fluorescence method. Using these data, we study the effect of charge exchange loss of fast ions with neutrals on E_r and partition of beam power. Figure 5 shows the E_r profile for low (A) and high (B) density NBI cases in the presence of neutral particle contributions. Open and closed data points in Fig. 5 are the experimental values. The charge exchange loss of fast ions can be effective in enhancing E_r, and the theoretical results approach to the experimental observations as the neutral density increases up to level of $10^{17}/m^3$ for low density and $10^{18}/m^3$ for high density. The required neutral density, which is used in the calculations to reproduce the radial electric field, seems to be higher than the experimental value. The partition rates versus the neutral density at the edge, n_{0s} is shown in Fig. 6. The radial electric fields at $\rho = 0.7$ and 0.9 are also plotted. It is important to discuss the trade off concerning on the energy balance.

4.3 Effect of anomalous particle loss

We study the effect of bipolar part of the anomalous particle loss on E_r on the basis of Eqs. (1) and (7). The local particle transport has been examined for NBI heated plasma[22] These observations show that the plasma density is $(1.5 \sim 2.5) \times 10^{19}/m^3$, the total particle flux is $(2 \sim 3) \times 10^{20}/s$ and the diffusion coefficient D is $(0.3 \sim 0.4)[m^2/s]$ at $\rho = 0.7$. Using these data, we evaluate the upper bound of the bipolar part of the anamalous coefficient $\alpha_A \simeq (5 \sim 10) \times 10^{18}/sm$ in Eq. (7). Figure 7 shows the radial profile of E_r for different values of α_A. (A) and (B) correspond to the low and high density cases, respectively. Open and closed data points are the experimental values. The inclusion of anomalous particle loss further enhances the radial electric field at the plasma edge. We should note that the results depend sensitively on the modelling of anomalous transports for both electrons and ions.

5 Formation of Positive Electric Field by ECH

In order to certify the clear effect of radial electric field on the confinement, it is necessary to develop a method which can control the radial electric field externally. Recently, the transition of electric field from the ion root to the electron root has been found in the superposition of ECH on NB heated plasmas in CHS[19] Here, we present a preliminary result on the formation of the positive radial electric field through enchancing the particle flux due to ECH and study its relation among resonance positions, power and injection modes[26]

The ripple top (bottom) of the magnetic field strength is located at high (low) field side near the mid-plane of the torus. Figure 8 shows the schematic drawing of resonance structure for the ripple top and bottom resonances at $r = 0.5a$. The injection power of ECH, P_{ECH} is up to 140kW and the density is adjusted below the cut-off density for second harmonic X−mode ECH. Typical plasma parameters in this experiment are summarized in Table 1. As a reference plasma, we choose the NB heated plasma without ECH by keeping the same line-averaged density as that for the plasma with ECH.

Figure 9 shows the radial profiles of $E_r(\rho)$ at 15ms after ECH is turned on for the reference plasma and those with P_{ECH}= 85kW and 140kW. Large positive electric field is observed in case of P_{ECH} = 140kW while E_r for the reference plasma and that with P_{ECH} = 85kW is almost zero or small negative value.

Figure 10 shows the observed radial electric field profiles in case of the ripple bottom resonance with P_{ECH}= 140kW. The theoretical result of E_r is also shown, where the following nonlinear diffusion type equation for E_r is used[27] :

$$\frac{2}{\rho^2 a^2}\frac{d}{d\rho}[\rho^2\hat{\eta}(E_r' - \frac{E_r}{\rho})] - \frac{1}{a^2}\frac{\partial\hat{\eta}}{\partial E_r}(E_r' - \frac{E_r}{\rho})^2 = e[\Gamma_i^{NC}(E_r) - \Gamma_e^{NC}(E_r) - \Gamma_{ECH}]. \quad (11)$$

Here , we assumed that ECH enhances only electron particle flux and the dependence of Γ_{ECH} on E_r is not taken into consideration. The factor $\hat{\eta}B^2$ can be represented by a coefficient of shear viscosity μ^{eff} with $\hat{\eta}B^2 = n_i m_i \mu^{eff}$ (μ^{eff} is assumed to be constant parameter). Disagreement between the observation and theoretical result without viscosity term ($\mu^{eff} = 0$) is clear. But, the observed E_r profile is in well agreement with the theoretical result with $\mu^{eff} = 400 m^2 s^{-1}$.

6 Summary

We have discussed a theoretical model to determine selfconsistently the radial electric field and loss cone loss in heliotron/torsatron configurations under the influence of nonclassical ion and electron losses. Analysis was applied to the NBI heated and ECH plasmas in the CHS device. Comparison was made between the theoretical results and experimental observations.

For NBI heated plsama, the increased ion particle losses caused by the orbit loss, charge exchange loss of fast ions with neutrals, and bipolar part of anomalous transport make the radial electric field more negative compared to the prediction based on neoclassical theory. In ECH plasma, the enhanced particle flux due to the production of the

electrons accelerated perpendicularly to the magnetic field by ECH results in the charge of electric field.

In general, the particle and energy balance are strongly influenced by an anomalous transport and induced transport. We discussed a simplified model to explain the experimental observations. Role of the radial electric field on confinement under the influence of anomalous and rf-induced transport needs further investigations theoretically and experimentally in order to conclude the overall trade-off on the energy balance.

Acknowledgements

We would like to acknowledge all members of torus experiment group in NIFS for useful discussions on experimental data. We also greatly appreciates Professor S. -I. Itoh for stimulating discussions.

References

[1] R. J. Groebner et al. : Phys. Rev. Lett. 64(1990) 3015.

[2] K. H. Burrell et al. : Phys. Fluids B2 (1990) 1405.

[3] R. J. Taylor et al. : Phys. Rev. Lett. 63 (1989) 2365.

[4] Y. Miura and JFT-2M Group : in 13th Int. Conf. on Plasma Physics and Controlled Nuclear Fusion Research (IAEA, Washington, 1990) Paper IAEA-CN-53/A-4-2.

[5] K. Toi et al. : in 14th Int. Conf. on Plasma Physics and Controlled Nuclear Fusion Research (IAEA, Würzburg, 1992) Paper IAEA-CN-56/H-1-3.

[6] V. Erckmann et al. : Phys. Rev. Lett. 70 (1993) 2086.

[7] S. -I. Itoh and K. Itoh : Phys. Rev. Lett. 60 (1988) 2276.

[8] K. C. Shaing and E. C. Crume Jr. : Phys. Rev. Lett. 63 (1989) 2369.

[9] A. B. Hassam et al. : Phys. Rev. Lett. 66 (1991) 309.

[10] F. L. Hinton : Phys. Fluids B3 (1991) 696.

[11] J. G. Gorman and L. H. TH. Rietjents : Phys. Fluids 9 (1966) 2504.

[12] A. Mohri and M. Fujiwara : Nucl. Fusion 14 (1974) 67.

[13] WVII-A Team and NBI Team : in Poc. 11th European Conf. on Controlled Fusion and Plasma Physics (Aachen, 1983) Vol. 7D, Part I, p.199.

[14] K. Kondo et al. : in Proc. of Int. Conf. on Plasma Physics, Innsbruck, 1992, Vol. 16C, Part I, p.529.

[15] H. Renner, W7AS Team, NBI Group, ICF Group, ECRH Group : Plasma Phys. Contr. Fusion 31 (1989) 1579.

[16] S. C. Aceto et al. : Rev. Sci. of Int. Conf. on Plasma Physics, Innsbruck, 1992, Vol. 16C, Part I, p.529.

[17] K. Matsuoka et al. : Plasma Physics and Controlled Nuclear Fusion Research, 1988, Nice (IAEA Vienna 1989) Vol. II p.411.

[18] K. Ida, H. Yamada, H. Iguchi et al. : Phys. Fluids B3 (1991) 515, B4 (1991) 1360.

[19] H. Idei, K. Ida, H. Sanuki et al. : Phys. Rev. Lett. 71 (1993) 2220.

[20] H. Sanuki, K. Itoh, K. Ida and S.-I. Itoh : J. Phys. Soc. Jpn. 60 (1991) 3698.

[21] H. Sanuki, I. Itoh and S.-I. Itoh : J. Phys. Soc. Jpn. 62 (1993) 123.

[22] H. Iguchi et al. : in Proc. 1992 Int. Conf. on Plasma Physics and 19th European Conf. on Controlled Fusion and Plasma Physics (Innsbruck, Austria) Part I p.517.

[23] K. Uchino et al. : J. of Nuclear Materials 196 – 198 (1992) 210.

[24] K. Itoh, H. Sanuki, J. Todoroki et al. : Phys. Fluids B3 (1991) 1294.

[25] S. Okamura et al. : in 14th Int. Conf. on Plasma Physics and Controllef Nuclear Fusion Research (IAEA, Würzburg, 1992) IAEA-Cn-56/C-2-4.

[26] H. Idei, K. Ida, H. Sanuki et al. : in preparation for publication.

[27] H. Maassberg et al. : Phys. Fluids B5 (1993) 3627.

Figure Captions

Fig. 1 A flow chart of several topics associated with E_r and/or E_r' involved in the persent analysis.

Fig. 2 Typical process involved in the recent CHS experiments.

Fig. 3 Radial profiles of density, ion and electron temperatures (n, T_i and T_e) for low (A) and high (B) NBI discharges in CHS device. Radial electric field profiles for these discharges are also shown, together with neoclassical results.

Fig. 4 Radial electric field determined selfconsistetly under the influence of orbit loss for low (A) and high (B) density cases. In (A), the results (a) to (c) represent the radial profile of E_r in case of (a) without orbit loss, (b) with orbit loss (W_b =18keV) and (c) with orbit loss (W_b = 12keV) for loss density case. The radial profiles of E_r in case of (a) $W_b = 0$, (b) W_b = 36keV, (c) W_b = 18keV, and (d) W_b = 12keV are shown in (B) for high density case.

Fig. 5 Radial electric fields in the presence of neutral particle contribution. (A) and (B) correspond to the low and high density cases. Experimental observations, which are quoted from ref. 21. In (A), (a) $n_{os} = 0$, (b) $4.0 \times 10^{16}/m^3$, (c) $8.0 \times 10^{16}/m^3$, (d) $2.0 \times 10^{17}/m^3$, and (e) $5.0 \times 10^{17}/m^3$. In (B), (a) $n_{os} = 0$, (b) $1.5 \times 10^{17}/m^3$, (c) $4.0 \times 10^{17}/m^3$, (d) $8.0 \times 10^{17}/m^3$, and (e) $1.5 \times 10^{18}/m^3$.

Fig. 6 Partition rates among the shine through (η_{st}), charge exchange loss (η_{cx}) and bulk heating (η_{bh}) versus the neutral density, n_{os}, for low (A) and high (B) densities. Radial electric fields at $\rho = 0.7$ and 0.9 are also shown.

Fig. 7 Radial profile of E_r for several values of α_A ; (a) $\alpha_A = 0$, (b) $5 \times 10^{18}/sm$, (c) $1.0 \times 10^{19}/sm$ and $n_{os} = 5.0 \times 10^{17}/m^3$ in (A) and $1.5 \times 10^{18}/m^3$ in (B) are used. The results for low density and high density are shown in (A) and (B). Open and closed data points are the experimental results.

Fig. 8 Shematic drawing of resonance structure for ripple top and bottom resonances at $r = 0.5a$.

Fig.9 Radial profiles of $E_r(\varrho)$ at 15ms after ECH is turned on for refernce plasma and those with P_{ECH} = 85kW and 140kW.

Fig. 10 Observed radial electric field profile in case of ripple bottom resonance with P_{ECH} = 140kW. Theoretical results is also shown.

Table I Machine and plasma parameters for NBI and NBI + ECH experiments

parameter		NBI + ECH	NBI (Low, High)
Magnetic configuration		Heliotron/Torsatron	
Major radius	R	100cm	
averaged minor radius	a	20cm	
toroidal field	$B_t(0)$	0.75T~0.93T	1T~2T
inverse aspect ratio	$\varepsilon_t(a)$	0.2	
helical ripple	$\varepsilon_h(a)$	0.29	
rotational transform	$\iota(0)$	0.3	
rotational transform	$\iota(a)$	1.2	
NBI/ECH Power	P_{NBI}	1MW	1MW
	P_{ECH}	Max140kW(2nd)	
NBI direction		tangential	tangential (variable)
electron density	$n_e(0)$	$\sim 1.0 \times 10^{13}/cm^3$	$1.8, 5.6 \times 10^{13}/cm^3$
electron temperature	$T_e(0)$	0.39keV	0.3, 0.2keV
ion temperature	$T_i(0)$	0.18keV	0.2, 0.18keV
electric Field (maximum)	$E_{r,max}$	$+40V/cm$ (at $r/a \sim 0.8$)	$-50, -120V/cm$ (at $r/a \sim 0.8$)

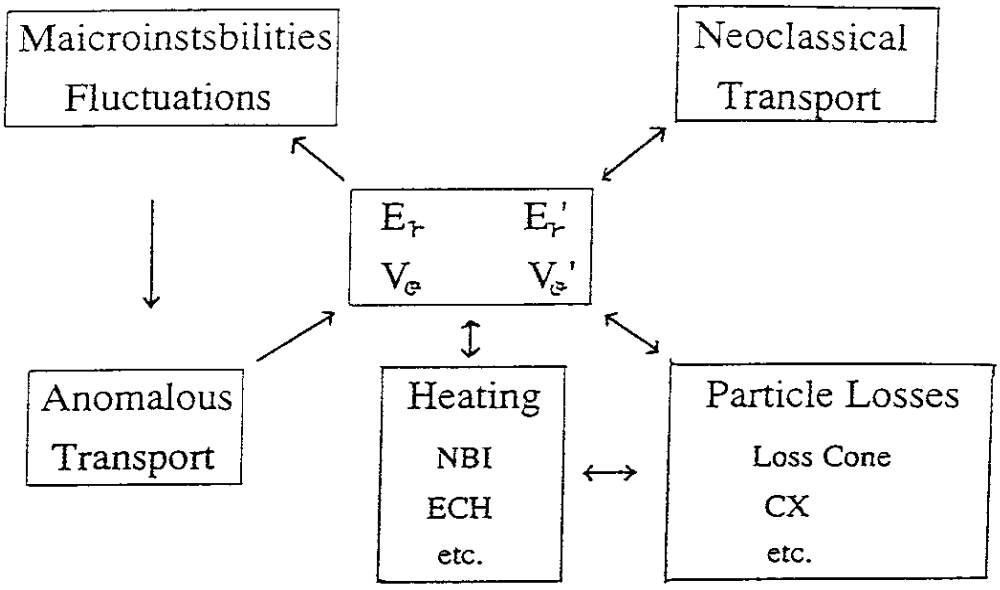
Maicroinstsbilities
Fluctuations
Neoclassical
Transport
E_r E_r'
V_θ V_θ'
Anomalous
Transport
Heating
NBI
ECH
etc.
Particle Losses
Loss Cone
CX
etc.

Fig.1

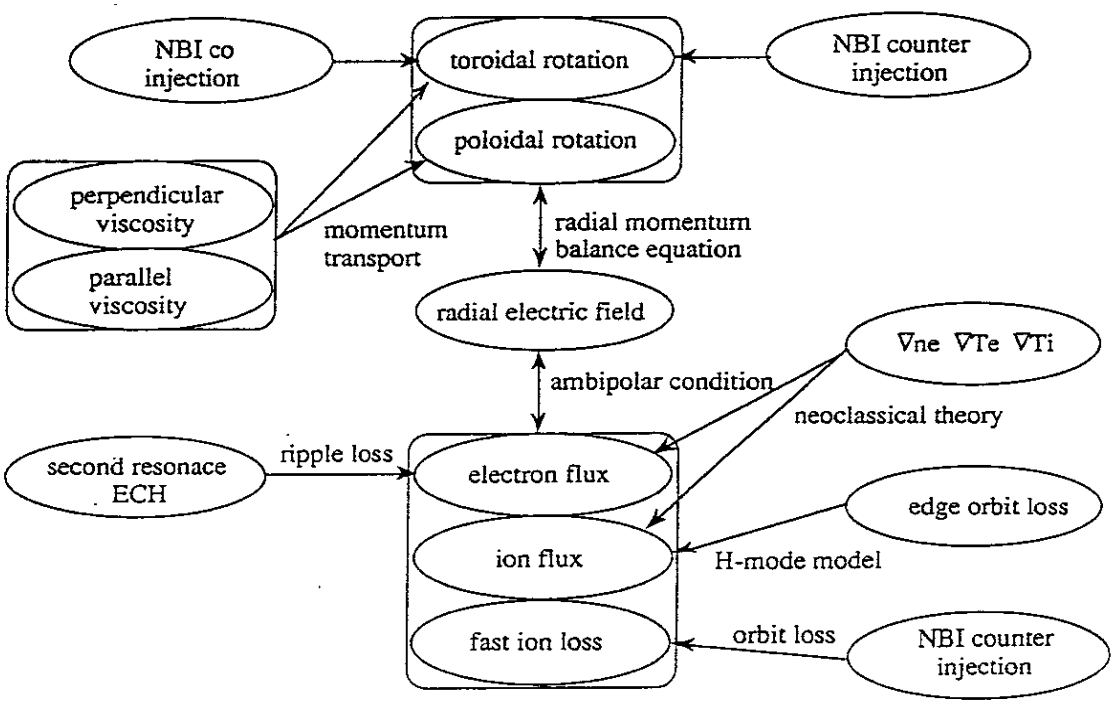
NBI co injection
toroidal rotation
NBI counter injection
poloidal rotation
perpendicular viscosity
parallel viscosity
momentum transport
radial momentum balance equation
radial electric field
∇ne ∇Te ∇Ti
ambipolar condition
neoclassical theory
second resonace ECH
ripple loss
electron flux
edge orbit loss
ion flux
H-mode model
fast ion loss
orbit loss
NBI counter injection

Fig.2

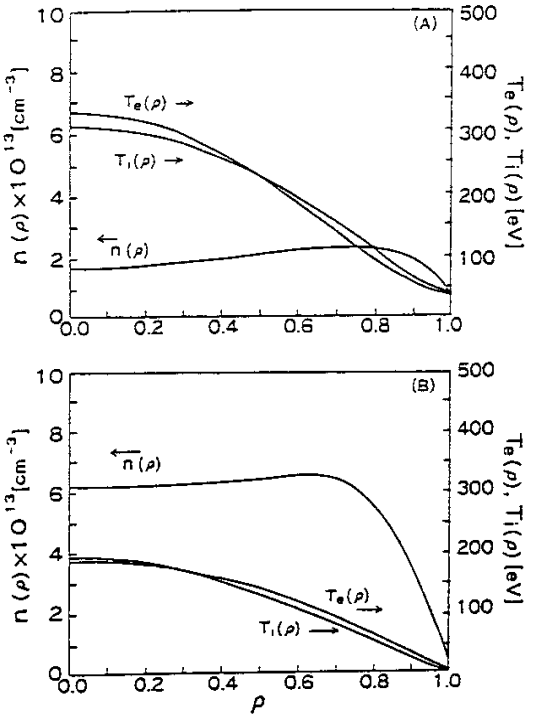
(A)
(B)
$T_e(\rho)$
$T_i(\rho)$
$\overleftarrow{n}(\rho)$
$n(\rho)\times10^{13}$[cm^{-3}]
$T_e(\rho)$, $T_i(\rho)$ [eV]
ρ

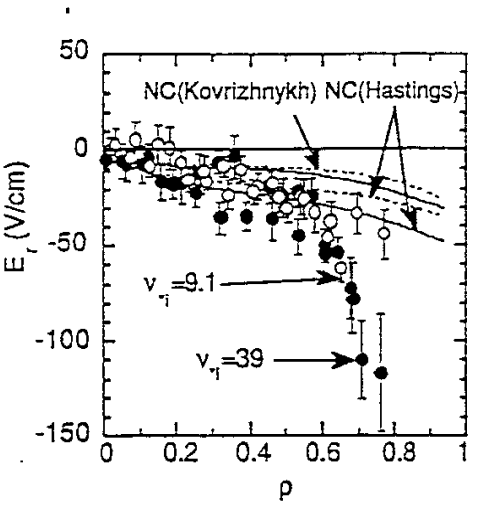
NC(Kovrizhnykh)
NC(Hastings)
ν_{*i}=9.1
ν_{*i}=39
E_r (V/cm)
ρ

Fig.3

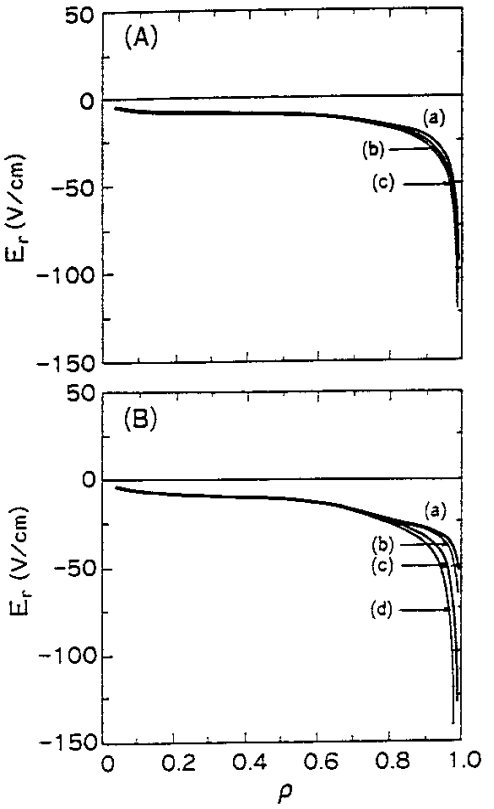
(A)
(B)
(a)
(b)
(c)
(d)
E_r (V/cm)
ρ

Fig.4

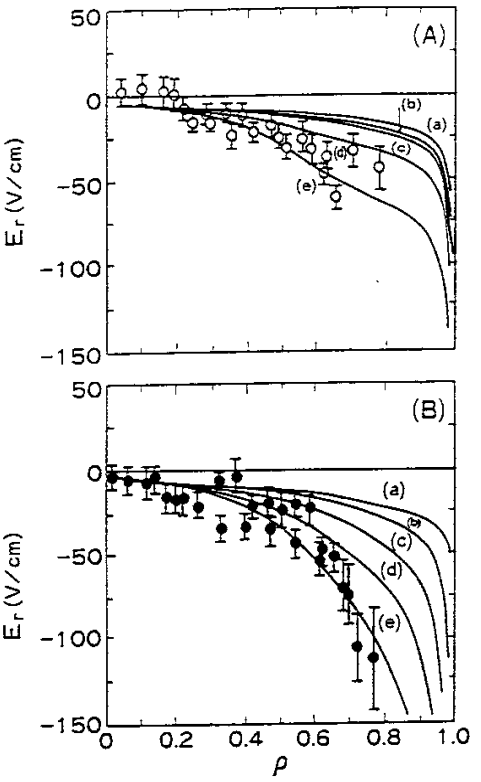
(A)
(B)
(a)
(b)
(c)
(d)
(e)
E_r (V/cm)
50
0
−50
−100
−150
0
0.2
0.4
0.6
0.8
1.0
ρ

Fig.5

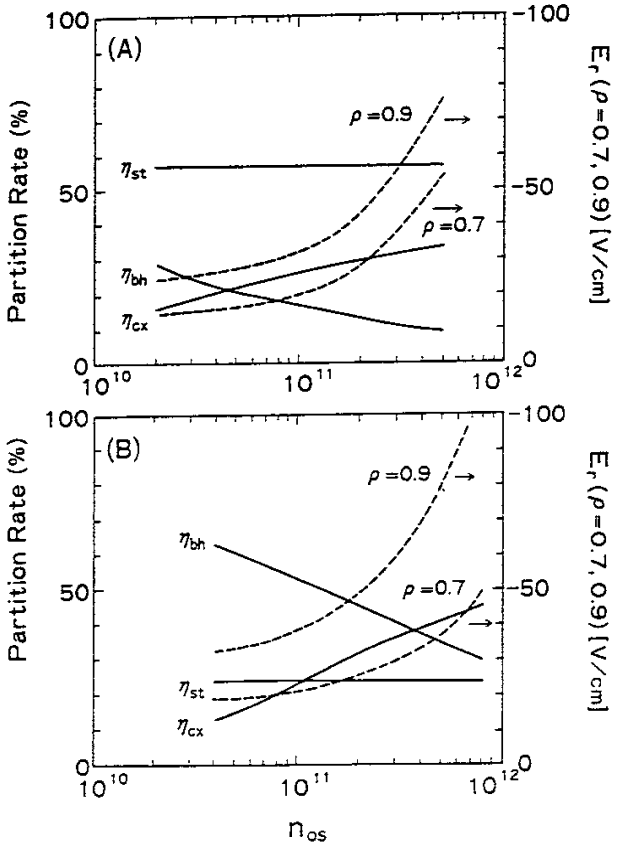
(A)
(B)
Partition Rate (%)
100
50
0
η_{st}
η_{bh}
η_{cx}
ρ =0.9
ρ =0.7
−100
−50
0
E_r (ρ=0.7, 0.9) [V/cm]
10^{10}
10^{11}
10^{12}
n_{os}

Fig.6

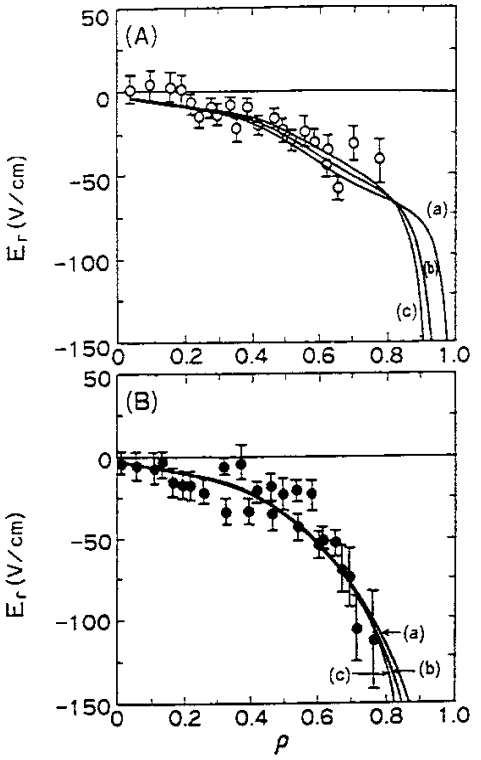
(A)
(B)
E_r (V/cm)
50
0
-50
-100
-150
0
0.2
0.4
0.6
0.8
1.0
(a)
(b)
(c)
ρ

Fig.7

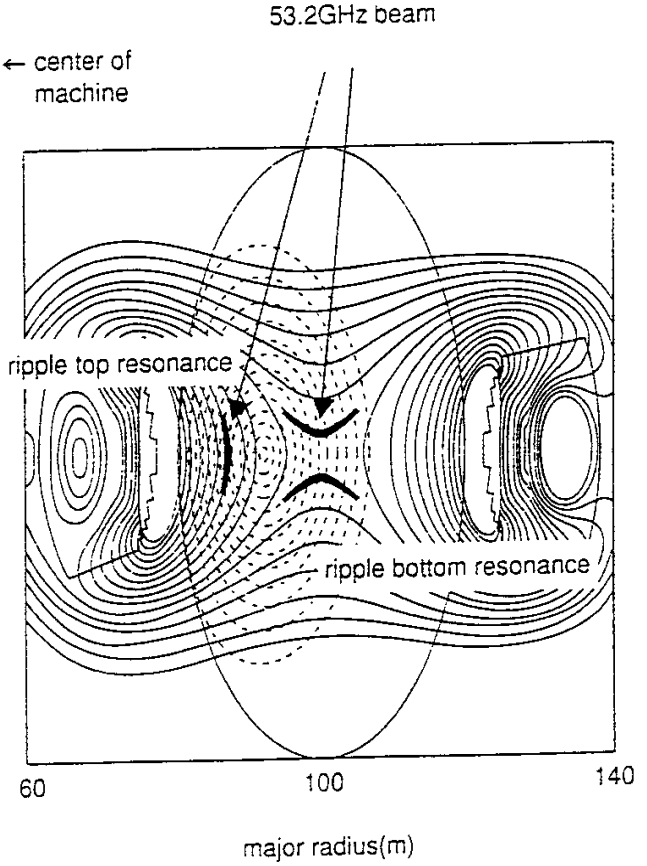
53.2GHz beam
← center of machine
ripple top resonance
ripple bottom resonance
60
100
140
major radius(m)

Fig.8

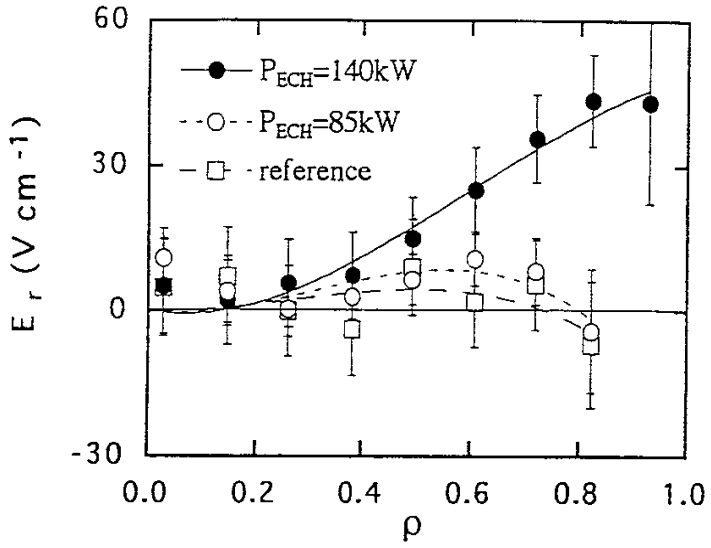
60
30
0
-30
E_r (V cm^{-1})
P_{ECH}=140kW
P_{ECH}=85kW
reference
0.0
0.2
0.4
0.6
0.8
1.0
ρ

Fig.9

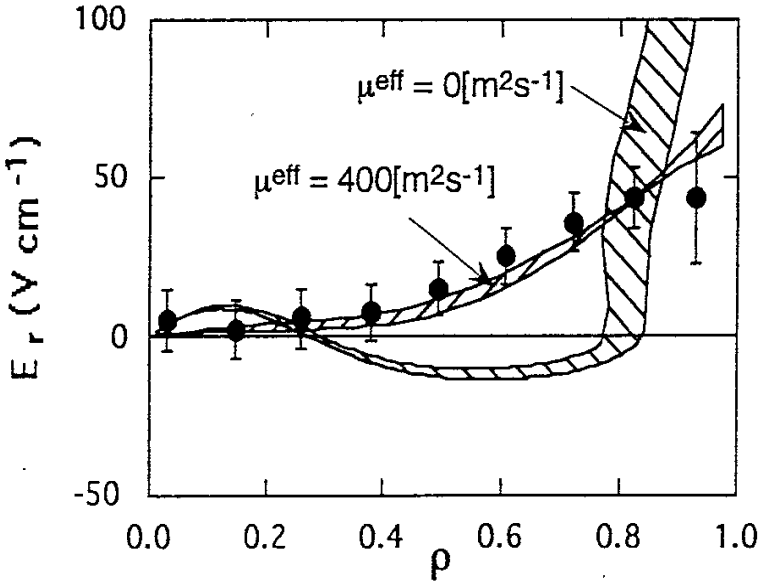
100
50
0
-50
E_r (V cm^{-1})
μ^{eff} = 0[m^{2}s^{-1}]
μ^{eff} = 400[m^{2}s^{-1}]
0.0
0.2
0.4
0.6
0.8
1.0
ρ

Fig.10

Recent Issues of NIFS Series

NIFS-241 K. Ida, Y.Miura, T. Matsuda, K. Itoh and JFT-2M Group, *Observation of non Diffusive Term of Toroidal Momentum Transport in the JFT-2M Tokamak;* Aug. 1993

NIFS-242 O.J.W.F. Kardaun, S.-I. Itoh, K. Itoh and J.W.P.F. Kardaun, *Discriminant Analysis to Predict the Occurrence of ELMS in H-Mode Discharges;* Aug. 1993

NIFS-243 K. Itoh, S.-I. Itoh, A. Fukuyama, *Modelling of Transport Phenomena;* Sep. 1993

NIFS-244 J. Todoroki, *Averaged Resistive MHD Equations;* Sep. 1993

NIFS-245 M. Tanaka, *The Origin of Collisionless Dissipation in Magnetic Reconnection;* Sep. 1993

NIFS-246 M. Yagi, K. Itoh, S.-I. Itoh, A. Fukuyama and M. Azumi, *Current Diffusive Ballooning Mode in Seecond Stability Region of Tokamaks;* Sep. 1993

NIFS-247 T. Yamagishi, *Trapped Electron Instabilities due to Electron Temperature Gradient and Anomalous Transport;* Oct. 1993

NIFS-248 Y. Kondoh, *Attractors of Dissipative Structure in Three Disspative Fluids;* Oct. 1993

NIFS-249 S. Murakami, M. Okamoto, N. Nakajima, M. Ohnishi, H. Okada, *Monte Carlo Simulation Study of the ICRF Minority Heating in the Large Helical Device;* Oct. 1993

NIFS-250 A. Iiyoshi, H. Momota, O. Motojima, M. Okamoto, S. Sudo, Y. Tomita, S. Yamaguchi, M. Ohnishi, M. Onozuka, C. Uenosono, *Innovative Energy Production in Fusion Reactors;* Oct. 1993

NIFS-251 H. Momota, O. Motojima, M. Okamoto, S. Sudo, Y. Tomita, S. Yamaguchi, A. Iiyoshi, M. Onozuka, M. Ohnishi, C. Uenosono, *Characteristics of D-^{3}He Fueled FRC Reactor: ARTEMIS-L,* Nov. 1993

NIFS-252 Y. Tomita, L.Y. Shu, H. Momota, *Direct Energy Conversion System for D-^{3}He Fusion,* Nov. 1993

NIFS-253 S. Sudo, Y. Tomita, S. Yamaguchi, A. Iiyoshi, H. Momota, O. Motojima,

M. Okamoto, M. Ohnishi, M. Onozuka, C. Uenosono,
Hydrogen Production in Fusion Reactors, Nov. 1993

NIFS-254 S. Yamaguchi, A. Iiyoshi, O. Motojima, M. Okamoto, S. Sudo, M. Ohnishi, M. Onozuka, C. Uenosono,
Direct Energy Conversion of Radiation Energy in Fusion Reactor, Nov. 1993

NIFS-255 S. Sudo, M. Kanno, H. Kaneko, S. Saka, T. Shirai, T. Baba,
Proposed High Speed Pellet Injection System "HIPEL" for Large Helical Device
Nov. 1993

NIFS-256 S. Yamada, H. Chikaraishi, S. Tanahashi, T. Mito, K. Takahata, N. Yanagi, M. Sakamoto, A. Nishimura, O. Motojima, J. Yamamoto, Y. Yonenaga, R. Watanabe,
Improvement of a High Current DC Power Supply System for Testing the Large Scaled Superconducting Cables and Magnets; Nov. 1993

NIFS-257 S. Sasaki, Y. Uesugi, S. Takamura, H. Sanuki, K. Kadota,
Temporal Behavior of the Electron Density Profile During Limiter Biasing in the HYBTOK-II Tokamak; Nov. 1993

NIFS-258 K. Yamazaki, H. Kaneko, S. Yamaguchi, K.Y. Watanabe, Y.Taniguchi, O.Motojima, LHD Group,
Design of Central Control System for Large Helical Device (LHD); Nov. 1993

NIFS-259 S. Yamada, T. Mito, A. Nishimura, K. Takahata, S. Satoh, J. Yamamoto, H. Yamamura, K. Masuda, S. Kashihara, K. Fukusada, E. Tada,
Reduction of Hydrocarbon Impurities in 200L/H Helium Liquefier-Refrigerator System; Nov. 1993

NIFS-260 B.V.Kuteev,
Pellet Ablation in Large Helical Device; Nov. 1993

NIFS-261 K. Yamazaki,
Proposal of "MODULAR HELIOTRON': Advanced Modular Helical System Compatible with Closed Helical Divertor; Nov. 1993

NIFS-262 V.D.Pustovitov,
Some Theoretical Problems of Magnetic Diagnostics in Tokamaks and Stellarators; Dec. 1993

NIFS-263 A. Fujisawa, H. Iguchi, Y. Hamada
A Study of Non-Ideal Focus Properties of 30° Parallel Plate Energy Analyzers; Dec. 1993

NIFS-264 K. Masai,

Nonequilibria in Thermal Emission from Supernova Remnants; Dec. 1993

NIFS-265 K. Masai, K. Nomoto,
X-Ray Enhancement of SN 1987A Due to Interaction with its Ring-like Nebula; Dec. 1993

NIFS-266 J. Uramoto
A Research of Possibility for Negative Muon Production by a Low Energy Electron Beam Accompanying Ion Beam; Dec. 1993

NIFS-267 H. Iguchi, K. Ida, H. Yamada, K. Itoh, S.-I. Itoh, K. Matsuoka, S. Okamura, H. Sanuki, I. Yamada, H. Takenaga, K. Uchino, K. Muraoka,
The Effect of Magnetic Field Configuration on Particle Pinch Velocity in Compact Helical System (CHS); Jan. 1994

NIFS-268 T. Shikama, C. Namba, M. Kosuda, Y. Maeda,
Development of High Time-Resolution Laser Flash Equipment for Thermal Diffusivity Measurements Usting Miniature-Size Specimens; Jan. 1994

NIFS-269 T. Hayashi, T. Sato, P. Merkel, J. Nührenberg, U. Schwenn,
Formation and 'Self-Healing' of Magnetic Islands in Finite-β Helias Equilibria; Jan. 1994

NIFS-270 S. Murakami, M. Okamoto, N. Nakajima, T. Mutoh,
Efficiencies of the ICRF Minority Heating in the CHS and LHD Plasmas; Jan. 1994

NIFS-271 Y. Nejoh, H. Sanuki,
Large Amplitude Langmuir and Ion-Acoustic Waves in a Relativistic Two-Fluid Plasma; Feb. 1994

NIFS-272 A. Fujisawa, H. Iguchi, A. Taniike, M. Sasao, Y. Hamada,
A 6MeV Heavy Ion Beam Probe for the Large Helical Device; Feb. 1994

NIFS-273 Y. Hamada, A. Nishizawa, Y. Kawasumi, K. Narihara, K. Sato, T. Seki, K. Toi, H. Iguchi, A. Fujisawa, K. Adachi, A. Ejiri, S. Hidekuma, S. Hirokura, K. Ida, J. Koong, K. Kawahata, M. Kojima, R. Kumazawa, H. Kuramoto, R. Liang, H. Sakakita, M. Sasao, K. N. Sato, T. Tsuzuki, J. Xu, I. Yamada, T. Watari, I. Negi,
Measurement of Profiles of the Space Potential in JIPP T-IIU Tokamak Plasmas by Slow Poloidal and Fast Toroidal Sweeps of a Heavy Ion Beam; Feb. 1994

NIFS-274 M. Tanaka,
A Mechanism of Collisionless Magnetic Reconnection; Mar. 1994

NIFS-275 A. Fukuyama, K. Itoh, S.-I. Itoh, M. Yagi and M. Azumi,
Isotope Effect on Confinement in DT Plasmas; Mar. 1994

NIFS-276 R.V. Reddy, K. Watanabe, T. Sato and T.H. Watanabe,
Impulsive Alfven Coupling between the Magnetosphere and Ionosphere; Apr.1994

NIFS-277 J. Uramoto,
A Possibility of π^- Meson Production by a Low Energy Electron Bunch and Positive Ion Bunch; Apr. 1994

NIFS-278 K. Itoh, S.-I. Itoh, A. Fukuyama, M. Yagi and M. Azumi,
Self-sustained Turbulence and L-mode Confinement in Toroidal Plasmas II; Apr. 1994

NIFS-279 K. Yamazaki and K.Y.Watanabe,
New Modular Heliotron System Compatible with Closed Helical Divertor and Good Plasma Confinement; Apr. 1994

NIFS-280 S. Okamura, K. Matsuoka, K. Nishimura, K. Tsumori, R. Akiyama, S. Sakakibara, H. Yamada, S. Morita, T. Morisaki,. N. Nakajima, K. Tanaka, J. Xu, K. Ida, H. Iguchi, A. Lazaros, T. Ozaki, H. Arimoto, A. Ejiri, M. Fujiwara, H. Idei. O. Kaneko, K. Kawahata, T. Kawamoto, A. Komori, S. Kubo, O. Motojima, V.D. Pustovitov, C. Takahashi, K. Toi and I. Yamada,
High-Beta Discharges with Neutral Beam Injection in CHS, Apr; 1994

NIFS-281 K. Kamada, H. Kinoshita and H. Takahashi,
Anomalous Heat Evolution of Deuteron Implanted Al on Electron Bombardment ; May 1994

NIFS-282 H. Takamaru, T. Sato, K. Watanabe and R. Horiuchi,
Super Ion Acoustic Double Layer; May 1994

NIFS-283 O.Mitarai and S. Sudo
Ignition Characteristics in D-T Helical Reactors; June 1994

NIFS-284 R. Horiuchi and T. Sato,
Particle Simulation Study of Driven Magnetic Reconnection in a Collisionless Plasma; June 1994

NIFS-285 K.Y. Watanabe, N. Nakajima, M. Okamoto, K. Yamazaki, Y. Nakamura, M. Wakatani,
Effect of Collisionality and Radial Electric Field on Bootstrap Current in LHD (Large Helical Device); June 1994